Optimization, Evaluation and Comparison of Stator Topologies for Magnetically Levitated Fractional-Horsepower High-Speed PMSMs

Andreas J. PRÖLL*, Peter DIRNBERGER** and Wolfgang GRUBER*
* Institute of Electric Drives and Power Electronics, JKU Linz
Austria
** Linz Center of Mechatronics GmbH Linz
Austria

Abstract
High-speed electric drives are increasingly utilized in applications such as turbochargers, mechanical transmitters, and printed-circuit-board (PCB) drills due to their compactness and efficiency. This study focuses on the optimization and experimental validation of four different stator topologies for high-speed motors operating at speeds up to 200,000 rpm with a two-pole permanent magnet rotor. A multi-objective optimization process, based on finite element (FE) simulations and a genetic algorithm (NSGA-II), was conducted to minimize copper and iron losses, end winding length, material costs, and passive radial stiffness while maximizing efficiency. The optimized designs were subsequently validated through prototype construction and testing. The investigated stator topologies include slot-less designs with distributed and toroidal windings, as well as slotted designs with toroidal and concentric windings. Magnetic bearings are employed to reduce friction and extend service life, while constraints such as mechanical air gap and outer stator diameter are kept constant across all designs. The study also consider the influence of rotor magnet strength and material properties on efficiency and costs. Experimental validation involved run-down tests in a vacuum chamber to isolate stator iron losses from air friction and other losses. The results demonstrate good agreement between simulations and measurements. The findings provide valuable insights into trade-offs between efficiency, cost, and performance in high-speed motor design, offering practical guidelines for selecting suitable stator topologies for specific applications.

Keywords : High-Speed, Iron losses, Magnetic bearing, Stator topology, Testing, Simulation

1. Introduction

Advantages, e.g. low friction at high rotational speeds or wear-free operation, of electrical high-speed drives [1], [2] can be exploited in numerous applications. Examples in the literature range from turbo-chargers [3], mechanical transmitter [4] and turbo-compressor [5] to PCB drills [6]. Therefore, in prior art the characteristics of different high-speed machine-topologies have been studied [7], [8]. However, these studies often remain limited to simulation results. In this work, we optimize several potential stators to operate with the same two-pole high-speed (up to 200.000 rpm) permanent magnetic rotor. To solve this multi-objective optimization problems we use FE simulations. Thereafter four prototype motors are also built and their characteristics are verified by real performance on a test rig. However, the considered stator topologies are illustrated in Fig. 1.

2. Simulation and Optimization

This section presents the simulation and optimization process of the different stators, which is based on a genetic optimization algorithm (NSGA-II) implemented in SyMSpace [9]. The electric machine performance is computed using 2D FE software FEMM.

2.1. Requirements for High-speed Motors

The machines considered here are suitable for the textile industry, where high speeds but relatively low torques are required. The output power range is approximately 100 to 200 W for steady state operation. Of course, attention must be

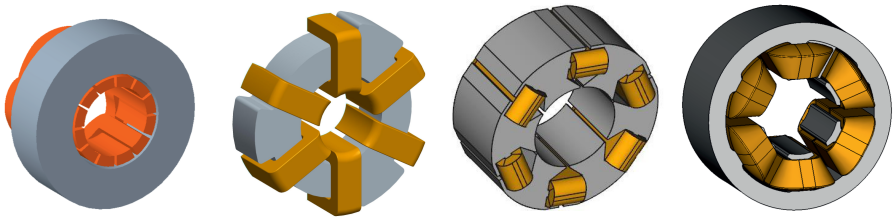

a) b) c) d)

Figure 1: Schematic images of stator topologies under investigation: slot-less type with stranded air-gap winding with a) distributed and b) toroidal coils as well as slotted type with standard (round) wires with c) toroidal and d) concentric coils.

paid to efficiency, as heat dissipation is often very limited in textile machines and low power consumption is demanded. AC losses play a major role in high-speed motors due to the high frequency of the rotor field. As a result, the pole pair number of the rotor magnet is defined as $p = 1$.

Proximity losses

$$P_{\text{prox}} \propto f^2 \cdot B^2 \cdot d^4 \cdot V, \tag{1}$$

where f is the frequency, B the magnetic flux density, d the diameter of the conductor and V the volume of the winding, are particularly important in the copper windings for air-coil stators (a) and (b) in Fig. 1. If the conductor diameter become too large, the rotor field generates considerable losses, which can represent a significant portion of all stator-losses. This is why so-called litz-wires are usually used. However, the individually insulated parallel conductors must be twisted with a defined pitch to avoid inducing circulating currents. The field displacement in the winding changes the calculation of proximity losses, which was taken into account in the FE simulation.

Magnetic bearings are used to minimize bearing friction and significantly and increase the service life at higher speeds. Another limitation are bending-critical natural frequencies of the shaft. For this optimizations, the axial length of the drive is taken into account in order to make sure to remain below the first natural bending frequency during operation.

2.2. Simulation Setup

All stators under consideration are operated with the same magnetic bearing system. This means that the geometric boundary conditions of the housing and the shape of the shaft, as well as the mechanical air gap need be same for all stators. The outer diameter of the stator is limited, to make sure it still fits into the housing.

Table 1: Optimization goals

Copper losses at rated point of operation	Minimize
Iron losses at rated point of operation	Minimize
Length of end windings	Minimize
Material costs (volumes of materials)	Minimize
Passive radial stiffness	Minimize
Overall efficiency	Maximize

In the optimization process several common constraints are set. Although the same rotor dimensions are used for all stator topologies, optimization showed that a weaker rotor magnet is advantageous for stators (c) and (d) in order to achieve good efficiency with limited stiffness and outer diameter of the stator. The other parameters defining each stator geometry are tunable for optimization. The same goals are set for each stator topology optimization and given in Table 1. The rather unusual fourth optimization objective of minimizing the passive destabilizing stiffness was included to reduce influence on the radial active magnetic bearings used to support the rotor shaft. The result of these multi-criterion optimizations are Pareto fronts [9]. Hence, these graphs give selection guidelines for choosing a proper stator topology.

However, the comparison is not entirely fair, because each stator topology could have an optimum where the geometry of the rotor magnet and the length of the laminated core are also different. The advantage, is that the subsequent measurement can be conducted with the same housing and shaft parts. This is relatively simpler and geometrically dependent losses (e.g. air friction) are similar for all stators.

©2025 The Japan Society of Mechanical Engineers

When designing the coils for the concentrated tooth coil winding (stator (d)), it turned out that the optimal wire is relatively thick and difficult to wind. For this reason, the three phases of this stator are connected in delta instead of star, which results in thinner wire. All other stator windings are star-connected, which is generally favourable avoiding circular currents.

Table 2: Optimization parameters for all drives

Inner diameter of stator iron	min. 14 mm
Outer diameter of stator geometry	max. 60 mm
Magnetization strength of magnet	two types possibly
Shape of the stator teeth	variable
Material of stator core	selected materials
Winding and coil parameters	variable

Table 3: Fixed design parameters for all drives

Length or stator iron and magnet	21 mm
Shaft outer diameter	12 mm
Mechanical air gap	0.6 mm
Material of stator core	defined materials
Supply voltage	50 V
Rotor speed	200 krpm
Output Power, typ.	150 W

2.3. Simulation Models and Results

Figure 2 clearly shows that the selected stator with distributed winding (a) is the smallest. However, the winding head must be taken into account, which represents a significant proportion of the total axial length. Although stators (a) and (b) must be manufactured with litz-wire, they are modeled as equivalent solid conductors in the simulation in order to keep the calculation time low. An NdFeB N42 was used as the rotor magnet. For stators (c) and (d), a plastic-bonded NeFeB magnet with $Br = 0.65\,T$ had to be used due to the smaller magnetic air gap (from the rotor magnet to the stator iron) in order to keep the radial installation space and the radial magnetic stiffness. Winding holders and insulation distances are taken into account in the simulation.

Table 4: Simulation results for all topologies

Parameter	Description	Unit	Stator (a) with NO20	Stator (a) with Megaperm	Stator (b) with SMC	Stator (c) with NO 20	Stator (d) with NO20
U_{s0}	No load EMF at 200 krmp	V_{rms}	18.9	18.9	17.9	16.9	15
$P_{Fe0,Stator}$	No load stator iron losses	W	15.7	8.3	14.9	8.8	9.6
P_{Cu}	Copper losses at load point (max torque)	W	5.6	5.3	6.6	9.9	9.2
η	efficiency at load point (max torque and speed)	%	94.4	96.5	94.2	94.7	94.6
s_r	magnetic radial stiffness load point	N/mm	3.86	3.86	1.85	1.52	1.05

For high-speed motors, it is generally recommended to use iron materials with very low iron loss coefficients. For example, Megaperm 40L and NO20 sheets are used for the stator (a), SMC (Soft magnetic composites) is used for stator (b) and NO20 sheets for the stators (c) and (d). Different materials are used to explore a wider variety of material behaviors.

3. Prototype Measurements

To verify simulation results, four prototype stators have been manufactured, commissioned and tested. A quasi-current-source inverter (QCSI) was used to drive the motors. This inverter topology is favorable for high speeds as it has low losses (at low currents) and enables low third harmonic distortion (THD) of the phase current [10]. Figure 3 shows a selection of the manufactured prototypes. The windings of stator (a) and (b) are directly penetrated by the rotating rotor field, therefore these stators are wound with litz-wire to keep proximity losses negligible compared to iron losses.

3.1. Test Rig Description

All stators are built in a complete drive with magnetic bearings and electronics and are placed into a vacuum chamber, which is equipped with gas-tight cable bushings and pressure measurement as shown in Fig. 4b [11]. The power consumption of the motor electronics can also be measured for a plausibility check.

©2025 The Japan Society of Mechanical Engineers

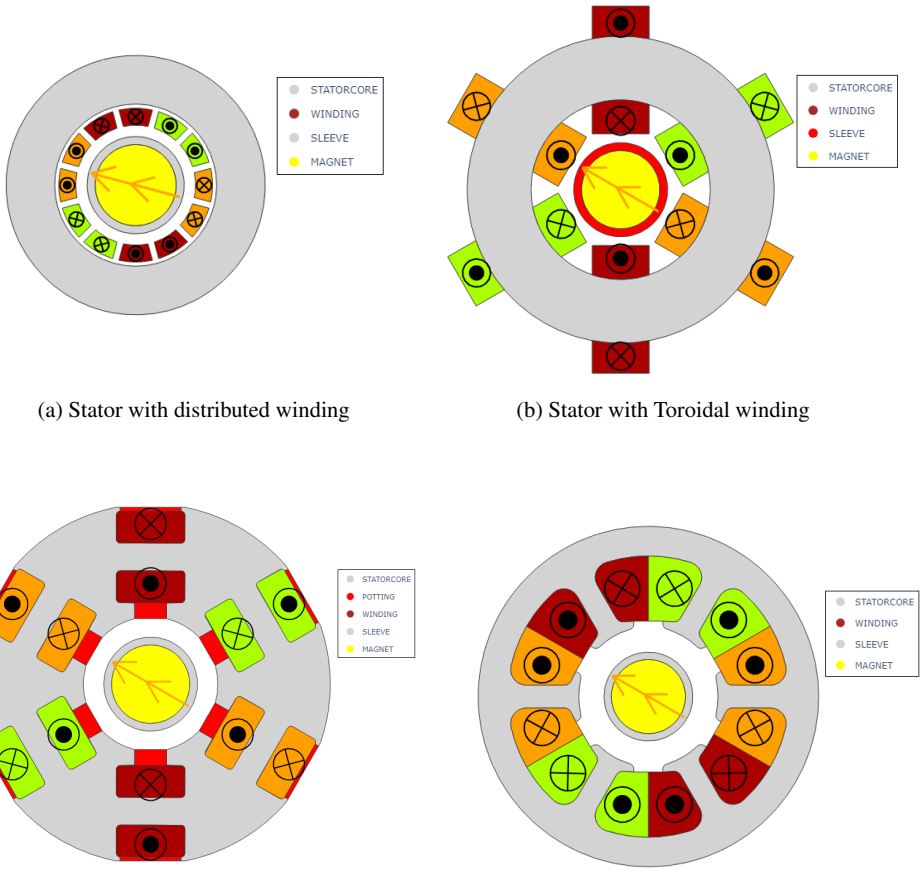

(a) Stator with distributed winding

(b) Stator with Toroidal winding

(c) Stator with Toroidal Pole-shoe winding

(d) Stator with Toothed coil winding

Figure 2: Simulation models in Symspace with optimized geometries.

The control unit enables of switching off the B6 bridge of the motor electronics after the shaft has run up to maximum speed. The magnetic bearings and speed measurement remain active. The speed of the out-running rotor can then be recorded over time.

3.2. Determination of No-Load Losses

The machine under test has a nominal torque in the double-digit mNm range. This makes it quite difficult to measure the power loss without influencing the system during the measurement. Measurements with a coupled load machine, where friction losses are known very precisely, are hardly possible at high speeds. It was therefore decided to measure the machine in standalone mode, i.e. to measure only the operating parameters without load. The no-load losses P_0 of the drive (without electronics) are composed as

$$P_0 = P_{v,stator} + P_{v,bear} + P_{v,rotor} + P_{v,air}. \tag{2}$$

Here, the rotor losses $P_{v,rotor}$ are practically insignificant due to the lack of rotor iron and the very homogeneous magnetic field in the rotor sleeve. The bearing losses $P_{v,bear}$ of the homopolar magnetic bearings are very small. They are very difficult to measure, which is why they are estimated with an upper limit of totally 2 W at highest speed using a 3D simulation, and thus be approximated using

$$P_{v,bear} < \left(\frac{n}{200000\,rpm}\right)^2 \cdot 2\,W. \tag{3}$$

The drive's main losses are the air friction losses, which are depending on the rotor geometry, the flow conditions and are usually proportional to the rotational speed by the power of three ($\propto \omega^3$). However, most interesting for this study are the

©2025 The Japan Society of Mechanical Engineers

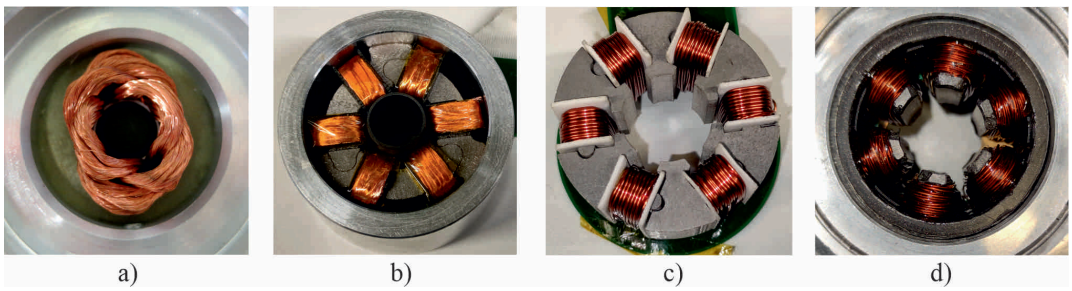

Figure 3: Manufactured prototype stators.

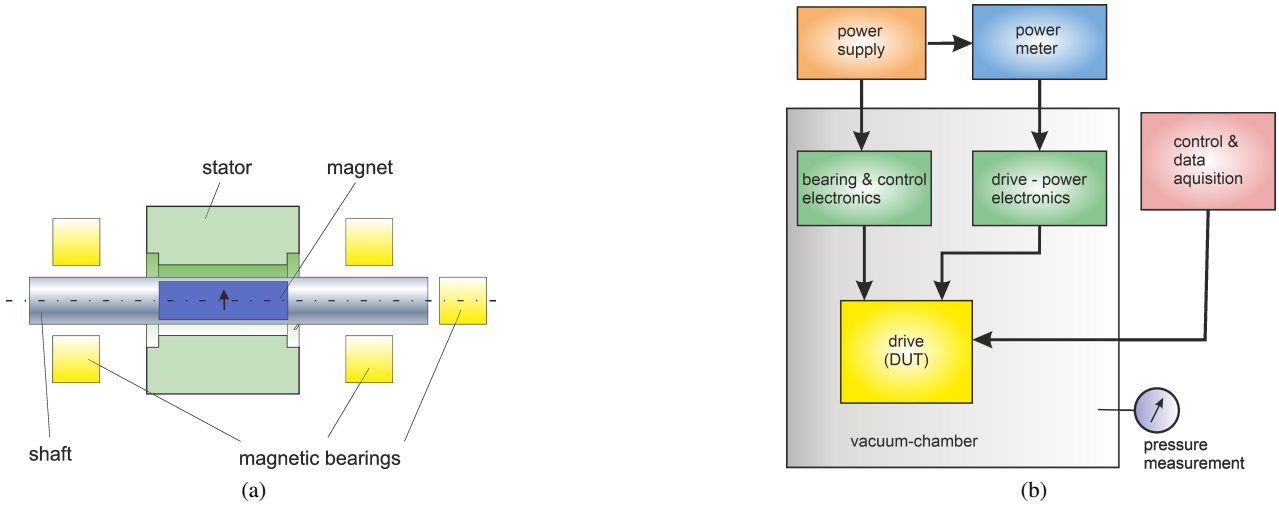

Figure 4: (a) Drive with magnetic bearings, (b) Test configuration with vacuum chamber

stator losses, which are composed of iron losses (hysteresis and eddy current losses) because they are often very difficult to measure. To separate the stator losses from the air friction losses, the drive is operated in a vacuum chamber. Switching off the drive electronics leads to negligible copper losses, as there is no current in the phases and the proximity effect in the wires caused by the rotor magnet is very small. In a so-called run-down test, the shaft decelerates due to power losses. Recording the speed curve over time allows calculation of the deceleration torque

$$T_{v,stator}(t) = J_{p,shaft} \cdot \dot{\omega}(t), \tag{4}$$

when the shaft's mass moment of inertia $J_{p,shaft}$ is known. For the time-dependent stator losses then follows

$$P_{v,stator}(t) = T_{v,stator}(t) \cdot \omega(t) = J_{p,shaft} \cdot \dot{\omega}(t) \cdot \omega(t). \tag{5}$$

3.3. Run-Down Measurements and Analysis

The speed curves from the run-out tests in the vacuum chamber are conveniently approximated by a 4^{th} order polynomial over time as

$$\omega(t) = a_0 + a_1 \cdot t + a_2 \cdot t^2 + a_3 \cdot t^3 + a_4 \cdot t^4. \tag{6}$$

Using its time derivative

$$\dot{\omega(t)} = b_0 + b_1 \cdot \omega + b_2 \cdot \omega^2 + b_3 \cdot \omega^3 \tag{7}$$

torque and power are determined with $\omega = \frac{n \cdot \pi}{30 \frac{s}{rpm}}$.

©2025 The Japan Society of Mechanical Engineers

In polynomial Eq. 7 b_0 should be inherently zero as well as because of vacuum the cubic part, representing the windage losses are negligible. In agreement with the Jordan loss formula in Eq. 8 [12], the calculated power is approximated by a 2^{nd} order polynomial

$$p_{Fe} = k_H \frac{f}{f_0} \frac{B^2}{B_0^2} + k_{EC} \left(\frac{f}{f_0} \frac{B}{B_0} \right)^2 , \tag{8}$$

where the linear coefficient k_H corresponds to hysteresis losses and the quadratic coefficient k_{EC} to eddy current losses.

With the knowledge of the iron loss terms, a new run-out test is started at ambient pressure. This allows determination of the cubic part of the power loss and thus the air friction in Fig. 5 (d).

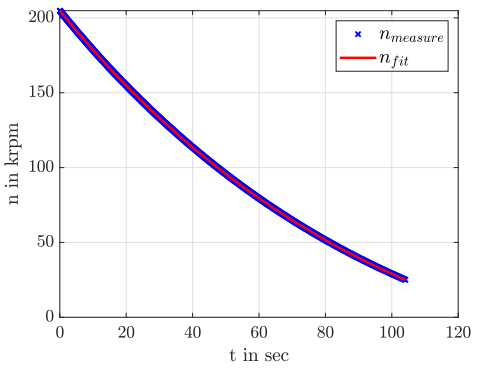

(a) Coasting measurement

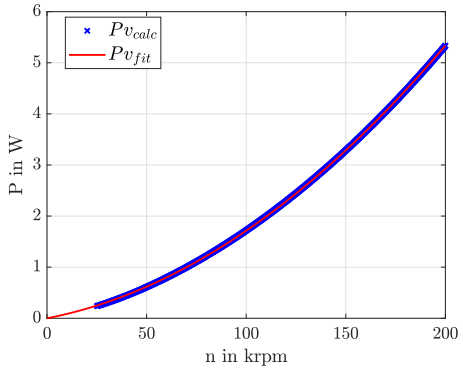

(b) Calculated power losses

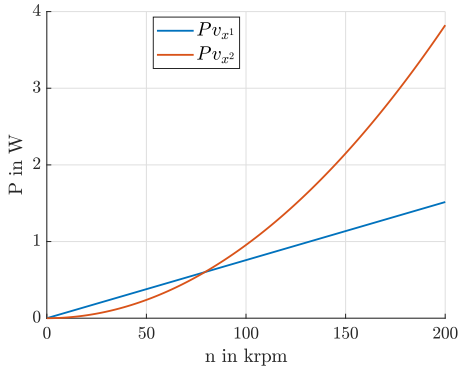

(c) Splitting up the power losses in vacuum

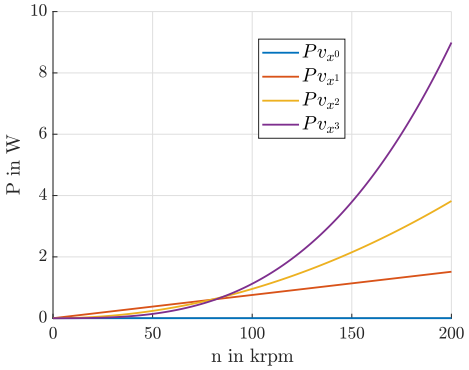

(d) Splitting up the power losses in ambient pressure

Figure 5: Analysis of run-down measurement of the stator (a) in vacuum.

3.4. Electromagnetic Force Measurement

During the run-out test, the phase voltages are measured with differential probes at a speed of 120 krpm (2 kHz). This can be used to determine the motor constant. In addition also differences in the phases, the phase angles and higher harmonics can be analyzed. Figure 6 shows the measured individual phase voltages. Table 6 gives a comparison with the simulation results.

©2025 The Japan Society of Mechanical Engineers

Table 5: Summary of measured values

Parameter	Description	Unit	Stator (a) with NO20	Stator (a) with Megaperm	Stator (b) with SMC	Stator (c) with NO 20	Stator (d) with NO20
$P_{v,hys}$	Stator iron hysteresis losses	W	2.8	1.15	4.9	3.1	4.3
$P_{v,eddy}$	Stator eddy current losses	W	6.8	4.65	5.7	6.5	8
$P_{airfric}$	Air-friction losses	W	10.6	10.8	10.7	14.3	14.1
$U_{s0,mean}$	EMF at 2kHz, phase to starpoint	Vrms	10.19	10.2	9.97	9.13	8.25

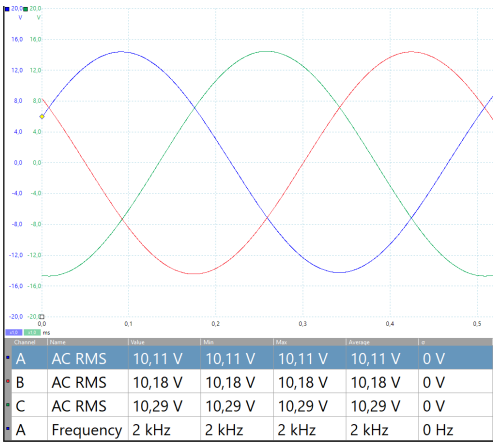

Figure 6: EMF measurement of Stator with distributed winding at 120krpm.

3.5. Results of all Measurements and Comparison to the Simulation

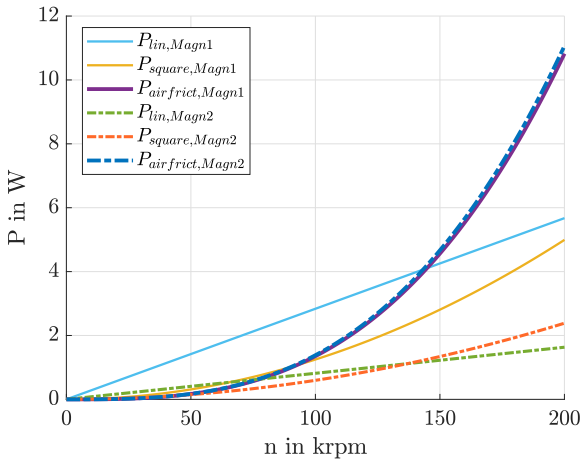

Figure 7: Verification of parameter fitting of run-down test, with equal air-friction, but different magnets.

Table 6: Comparison of simulation and measurement results

Parameter	Description	Unit	Stator (a) with NO20	Stator (a) with Megaperm	Stator (b) with SMC	Stator (c) with NO 20	Stator (d) with NO20
$P_{v,Fe,sim}$	Stator iron losses in simulation	W	15.7	8.3	14.9	8.8	10.9
$P_{v,Fe,meas}$	Stator iron losses from measurement	W	9.6	6.8	10.6	9.6	12.3
$U_{s0,sim}$	EMF at 200krpm in simulation	Vrms	18.9	18.9	17.9	16.9	15
$U_{s0,meas}$	EMF at 200krpm calc. from measurement	Vrms	16.7	16.8	16.5	14.85	13.6

©2025 The Japan Society of Mechanical Engineers

In comparison, the measured induced voltage (EMF) is around 10% lower for all stators than in the simulation. This can be explained by the fact that the stray fluxes in the axial direction are not considered in 2D simulation. Although the run-down tests produce clear coefficients, the values for iron losses differ in comparison to the simulation. Loss coefficients of the materials in FEM are often very imprecise or not specified at all, especially in the higher frequency range. Furthermore, the processing of the sheet metal also plays a crucial role. In a further optimization step, the measured loss coefficients could be incorporated back into the simulation in order to minimize the material uncertainties. However, almost identical air friction losses were found with similar air gap conditions. An additional test, in which a stator with the two geometrically identical shafts but with magnets of different strengths was measured, results in an almost identical cubic relationship between losses and speed, which is illustrated in Fig. 7. It can therefore be assumed that the proportions of the iron losses fit very well.

4. Conclusion and Outlook

Simulation models for four different stator topologies are implemented in order to carry out optimizations for the high-speed range. To verify simulation results, the different stators were set up and measured. Run-down test proved to be very suitable for separation the stator iron losses. In particular, when it is carried out in vacuum, because air friction, which accounts for most of the losses, is eliminated. All constructed stators show very similar performance but differ in the required installation space and manufacturing complexity. Future work should examine how variations in material loss coefficients affect the optimization results. In addition, copper losses should be measured, and skin, proximity, and eddy current losses should be separately identified.

References

[1] A. Binder and T. Schneider, *High-speed inverter-fed ac drives*, International Aegean Conference on Electrical Machines and Power Electronics, pp. 9–16, 2007.

[2] N. Bianchi, S. Bolognani, and L. F., "Potentials and limits of high-speed pm motors," *IEEE Transactions on Industry Applications*, vol. 40, no. 6, 1570–1578, 2004.

[3] M.-S. Lim, J.-M. Kim, Y.-S. Hwang, and J.-P. Hong, "Design of an ultra-high-speed permanent-magnet motor for an electric turbocharger considering speed response characteristics," *IEEE/ASME Transactions on Mechatronics*, vol. 22, no. 2, 774–784, 2017.

[4] K. Islam, S. Choi, Y.-K. Hong, and S. Kwak, "Design of high-power ultra-high-speed rotor for portable mechanical antenna drives," *IEEE Transactions on Industrial Electronics*, vol. 22, no. 1, p. 1, 2021.

[5] D. Krähenbühl, C. Zwyssig, H. Weser, and J. W. Kolar, "A miniature 500.000-r/min electrically driven turbocompressor," *IEEE Transactions on Industry Applications*, vol. 46, no. 6, 2459–2466, 2021.

[6] R. M. Kennel, *Ultra high speed drive with permanent magnet synchronous motors and hardware based field oriented control*, International Aegean Conference on Electrical Machines and Power Electronics, pp. 116–124, 2007.

[7] A. Gilson, F. Dubas, D. Depernet, and C. Espanet, *Comparison of high-speed pm machine topologies for electrically-assisted turbocharger applications*, 19th International Conference on Electrical Machines and Systems (ICEMS), pp. 1–5, 2016.

[8] A. Tenconi, S. Vaschetto, and A. Vigliani, "Electrical machines for high-speed applications: Design considerations and tradeoffs," *IEEE Transactions on Industrial Electronics*, vol. 61, no. 6, 3022–3029, 2014.

[9] S. Silber, W. Koppelstaetter, G. Weidenholzer, G. Segon, and G. Bramerdorfer, *Reducing development time of electric machines with symspace*, 8th International Electric Drives Production Conference (EDPC), pp. 1–5, 2016.

[10] F. Savi, M. D. N. D. Barater, M. Degano, C. Gerada, P. Wheeler, and G. Buticchi, "High-speed electric drives: A step towards system design," *IEEE Transactions on Industrial Electronics*, vol. 1, no. 1, pp. 10–21, 2020.

[11] A. Pröll, J. Sloupensky, P. Dirnberger, and W. Amrhein, *Testing the high speed shaft of a yarn spinning system with a magnetic bearing test device*, 16th International Symposium on Magnetic Bearings, pp. 1–5, 2018.

[12] C. Dobler, G. Bramerdorfer, G. Goldbeck, and W. Amrhein, "Studies of measurement un- certainties in the characterization of soft magnetic ma- terials and their impact on the electric machine perfor- mance prediction," *IEEE Energy Conversion Congress and Exposition (ECCE)*, vol. 1, no. 1, pp. 4411–4417, 2021.

©2025 The Japan Society of Mechanical Engineers